ACS APPLIED MATERIALS & INTERFACES
Research Article
www.acsami.org

Low-Temperature Conformal Atomic Layer Deposition of SiN_x Films Using Si_2Cl_6 and NH_3 Plasma

Rafaiel A. Ovanesyan,[†] Dennis M. Hausmann,[*,‡] and Sumit Agarwal[*,†]

[†]Chemical and Biological Engineering, Colorado School of Mines, Golden, Colorado 80401, United States
[‡]Lam Research Corporation, 11155 SW Leveton Drive, Tualatin, Oregon 97062, United States

ABSTRACT: A plasma-enhanced atomic layer deposition (ALD) process was developed for the growth of SiN_x thin films using Si_2Cl_6 and NH_3 plasma. At substrate temperatures ≤400 °C, we show that this ALD process leads to films with >95% conformality over high aspect ratio nanostructures with a growth per cycle of ~1.2 Å. The film growth mechanism was studied using in situ attenuated total reflection Fourier transform infrared spectroscopy. Our data show that on the SiN_x growth surface, Si_2Cl_6 reacts with surface $-NH_2$ groups to form surface −NH species, which are incorporated into the growing film. In the subsequent half cycle, radicals generated in the NH_3 plasma abstract surface Cl atoms, and restore an NH_x (x = 1,2)-terminated surface. Surface Si−N−Si bonds are also primarily formed during the NH_3 plasma half-cycle. The infrared data and Rutherford backscattering combined with hydrogen forward scattering shows that the films contain ~23% H atoms primarily incorporated as −NH groups.

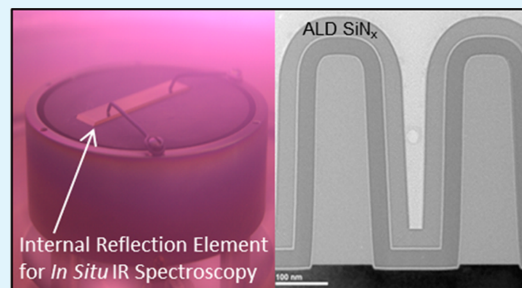

KEYWORDS: *silicon nitride, ALD, hexachlorodisilane, plasma, infrared*

1. INTRODUCTION

Atomic layer deposition (ALD) is a thin-film growth technique characterized by sequential, self-limiting, gas−solid reactions, which deposits a material layer by layer typically at a rate of ~1 Å/cycle.[1−3] The self-limiting nature of the surface reactions during ALD enables growth of highly conformal films over high-aspect-ratio nanostructures. Over the past two decades, a variety of materials have been deposited using ALD, which include metal oxides, nitrides, chalcogenides, and metals.[4−16] However, low-temperature growth of Si-based dielectric materials using ALD has been challenging. In particular, there are only a handful of studies that demonstrate ALD of SiN_x films at temperatures ≤400 °C—a requirement that is critical for applications of these films in semiconductor devices and photovoltaics. In semiconductor devices, the primary applications of SiN_x thin films include sidewall spacers, hard etch masks, and passivation layers.[17−20] In solar cells, SiN_x films are used as antireflection and passivation coatings,[21−23] and also as optical coatings in sensor equipment.[24] At the current <22 nm semiconductor technology node, plasma-assisted ALD technologies are beginning to replace the traditional plasma-enhanced chemical vapor deposition (PECVD) processes in applications that require conformal SiN_x layers with precisely controlled film thickness.[25] In particular, the shift to high-aspect-ratio FinFETs in modern semiconductor devices necessitates deposition of conformal SiN_x layers using ALD. However, the ALD of uniform, highly conformal, and dense SiN_x thin films over high-aspect-ratio structures at deposition temperatures ≤400 °C remains challenging.[26]

Previous research has shown that thermal ALD processes can be used to grow conformal SiN_x thin films. Traditionally, thermal ALD of SiN_x has been achieved using various chlorosilanes as the Si precursor, and primarily NH_3 or N_2H_4 as the N source. Briefly, Morishita et al. deposited SiN_x films using Si_2Cl_6 and N_2H_4 over a temperature range of 525−650 °C. The growth per cycle (GPC) for these SiN_x films was reported to be ~2.3 Å at an Si_2Cl_6 dose of ~1.4×10^7 L (1 L ≈ 1×10^6 Torr s), with a N/Si ratio of 1.39 and a refractive index of 1.8−2.1.[27] Later, Klaus et al. reported self-limiting SiN_x film growth using $SiCl_4$ and NH_3 at deposition temperatures of 423−623 °C with a GPC of 2.45 Å at an $SiCl_4$ exposure of up to 10^{10} L. The N/Si ratio was reported as ~1.35 with a refractive index of 2.01.[28] Nakajima et al. also used $SiCl_4$ and NH_3, combined with temperature cycling at 350 and 550 °C during the $SiCl_4$ and NH_3 half-cycles, respectively, and reported a GPC of ~1.75 Å.[29] Lee et al. demonstrated thermal ALD of SiN_x with both $SiCl_4$ and SiH_2Cl_2 with NH_3 at 500 °C. A GPC of ~1.3 and 1.2 Å was reported for the $SiCl_4$ and SiH_2Cl_2 processes, respectively, with both types of films being Si-rich with a N/Si ratio of ~1.[30] Zhu et al. used $SiCl_4$ and NH_3 at lower deposition temperatures over the range of 350−400 °C, after which the films were annealed in NH_3 ambient at 550 °C. However, the reported GPC was much lower, ~0.55 Å, most likely due to the lower deposition temperature.[31] Park et al. used Si_2Cl_6 and NH_3 as precursors over the deposition temperature range of 515−573 °C. The reported GPC was 2.4−2.8 Å at a Si_2Cl_6 dose of ~2×10^8 L. The deposited films had a N/Si ratio of ~1 with a refractive index of 1.7−1.8.[32]

Received: February 18, 2015
Accepted: April 30, 2015
Published: April 30, 2015

ACS Publications © 2015 American Chemical Society

DOI: 10.1021/acsami.5b01531
ACS Appl. Mater. Interfaces 2015, 7, 10806−10813

Although these previous thermal ALD processes for SiN_x have demonstrated viable growth rates and acceptable film properties, the deposition temperatures are generally too high for incorporation of these SiN_x films in modern semiconductor devices. These thermal ALD studies on SiN_x growth suggest that plasma and radical-assisted ALD processes may be required as a means of lowering the deposition temperatures to ≤400 °C.

A few studies on plasma-assisted ALD of SiN_x have also been reported in the literature. The N precursor half-cycle in these processes is typically an NH_3 plasma step since nitridation of Si at low temperatures is self-limiting.[33] Specifically, Goto et al. used SiH_2Cl_2 and NH_3 plasma to grow SiN_x films at deposition temperatures of 250−500 °C. The GPC was reported as ∼0.9 Å at an SiH_2Cl_2 dose of $\sim 5.4 \times 10^6$ L with a N/Si ratio of ∼1, and a refractive index of 1.6.[34] Yokoyama et al. also used SiH_2Cl_2 with a remote NH_3 plasma at deposition temperatures over the range of 250−400 °C. The reported GPC for these SiN_x films was 0.9 Å at an SiH_2Cl_2 exposure of $\sim 5.4 \times 10^6$ L, and the N/Si ratio was ∼1.1.[33] Later, Yokoyama et al. used SiH_2Cl_2 and NH_3 dissociated over a hot tungsten filament at a deposition temperature of 375 °C. The GPC for this SiN_x ALD process was ∼1 Å at an SiH_2Cl_2 exposure of $\sim 5.4 \times 10^6$ L, with a N/Si ratio of ∼1.1 and a refractive index of 1.9.[35] King used SiH_4 instead of a chlorinated silane precursor, and demonstrated that an N_2 plasma can be used for SiN_x ALD at deposition temperatures over the range of 250−400 °C.[25] The reactivity of SiH_4 at such low temperatures was attributed to the presence of dangling bonds on the surface after the N_2 plasma half-cycle. The reported GPC for this SiH_4-based ALD process was ∼2.5 Å, with a N/Si ratio of ∼1.2, and a relatively low refractive index of 1.75.[25] Jang et al. used $N(SiH_3)_3$—a precursor previously used for thermal CVD of SiN_x—combined with an NH_3 plasma for SiN_x ALD at temperatures over the range of 250−350 °C. The reported GPC in this low-temperature process was ∼0.65 Å at an $N(SiH_3)_3$ dose of $\sim 6 \times 10^4$ L, which was nearly 2 orders of magnitude lower than other chlorosilane-based SiN_x ALD processes. The refractive index of these SiN_x films was 1.8.[36] Thus, from these previous studies on plasma-assisted ALD of SiN_x, it is clear that self-limiting film growth occurs at GPC values and stoichiometries that are similar to those observed in thermal SiN_x ALD processes, but at substantially lower substrate temperatures. Therefore, plasma-assisted SiN_x ALD can potentially enable growth processes for next-generation semiconductor devices. However, the conformality and compositional uniformity of these films remains an issue during growth on high-aspect-ratio nanostructures.

In this article, we present a novel, self-limiting, plasma-assisted ALD process for the growth of SiN_x thin films with >95% conformality over high-aspect-ratio structures at substrate temperatures of 350−450 °C using Si_2Cl_6 and NH_3 plasma. The corresponding surface reactions during the Si_2Cl_6 and NH_3 plasma half-cycles were observed using in situ attenuated total reflection Fourier transform infrared (ATR-FTIR) spectroscopy.[37,38] These infrared studies were used to identify the surface reactive sites, and to elucidate the H incorporation mechanism in the deposited SiN_x films. In addition, the SiN_x films were characterized using ex situ techniques including transmission electron microscopy (TEM), Rutherford backscattering (RBS) combined with hydrogen forward scattering (HFS), and ellipsometry.

2. EXPERIMENTAL DETAILS

ALD Reactor and In Situ ATR-FTIR Spectroscopy Setup. The SiN_x films were deposited in an ALD reactor (see Figure 1), which was evacuated to a base pressure of $\sim 1 \times 10^{-7}$ Torr with a turbomolecular pump (Pfeiffer TMU-521 P) backed by a dry mechanical pump (Kashiyama NV60N-2). This ALD reactor was equipped with an in situ ATR-FTIR spectroscopy setup described previously.[37,39−43] Briefly, in this setup, an infrared beam from a commercial FTIR spectrometer (Nicolet 6700), was directed by a series of optics normally onto the tapered face of a trapezoidal 50 × 20 × 1 mm ZnSe internal reflection crystal (IRC) with the two short faces beveled at 45° (see Figure 1). The infrared beam was incident onto the flat face at an angle of 45°, which is greater than the angle for total internal reflection. The infrared beam underwent ∼25 internal reflections on the top and bottom faces of the crystal, after which it exited through the opposite 45° beveled edge, and was channeled through another set of optics to a liquid-N_2-cooled mercury cadmium telluride (MCT-A) detector. The ZnSe IRC, which was used as the deposition substrate, was clamped onto a substrate heater (Blue Wave Semiconductors), which also acted as the grounded electrode for the capacitively coupled plasma source (see Figure 1). The plasma source was radio frequency (rf) powered at 13.56 MHz. During ALD, the plate spacing between the grounded substrate and the top rf-powered electrode was kept at 3.5 cm.

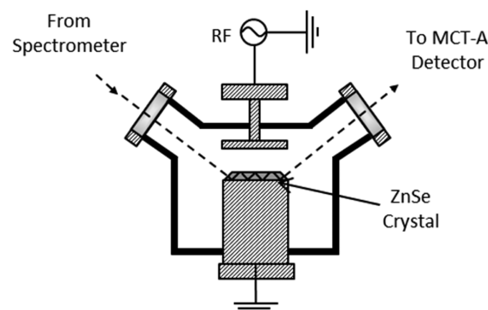

Figure 1. Schematic of the ALD reactor equipped with an in situ ATR-FTIR spectroscopy setup. The dashed line shows the infrared beam path from the spectrometer, through the ZnSe internal reflection crystal, and into the MCT-A detector.

ZnSe was used as the IRC because it is transparent in the infrared up to ~ 700 cm^{-1} at temperatures >500 °C, which allowed us to observe most of the relevant vibrational modes during the growth of the SiN_x films. To ensure that we were studying SiN_x ALD on a relevant growth surface, prior to recording data for the SiN_x ALD process, we coated the ZnSe IRC with a thin amorphous hydrogenated SiN_x (*a*-SiN_x:H) film grown at 350 °C using PECVD. During the PECVD process, the flow rate of SiH_4/Ar (1% SiH_4, 99% Ar) and NH_3 was 200 and 10 standard cm^3/min (sccm), respectively, at a chamber pressure of 100 mTorr and 100 W rf power. The PECVD *a*-SiN_x:H film was then coated with an ultrathin SiN_x film grown using five complete ALD cycles at the conditions relevant to the particular experiment to completely erase the memory of the underlying ZnSe substrate on the growth process.

ALD Process and In Situ ATR-FTIR Data Collection. The plasma-assisted SiN_x ALD process consisted of sequential, two-step alternating cycles where the first half-cycle was Si_2Cl_6 exposure, and the second half-cycle was NH_3 plasma exposure, separated by Ar purge steps (see Figure 2). All process gases were delivered through mass flow controllers via pneumatically actuated valves controlled through LabView. Si_2Cl_6 (Sigma-Aldrich, 96%) was delivered using a fill-and-release method where the fill volume was ∼10 cm^3. The Si_2Cl_6 ampule was heated to 70 °C, while the fill volume and the delivery line to the ALD reactor were maintained at 45 °C to prevent Si_2Cl_6 condensation. During each half-cycle, the Si_2Cl_6 fill time was 5 s, and the release time was 30 s, resulting in a maximum chamber pressure ∼70 mTorr. The

DOI: 10.1021/acsami.5b01531
ACS Appl. Mater. Interfaces 2015, 7, 10806−10813

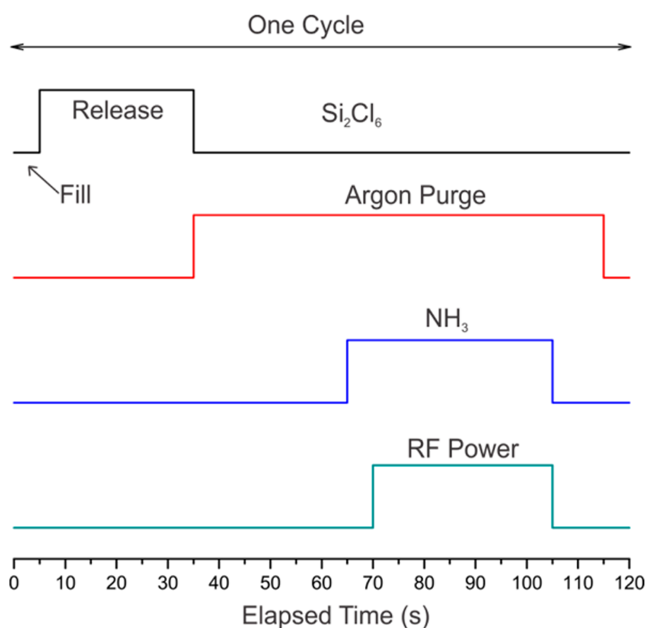

Figure 2. Schematic showing the gas pulsing sequence during plasma-assisted ALD of SiN_x.

Si_2Cl_6 cycle was followed by a 30 s Ar purge step at 100 sccm resulting in a chamber pressure of 80 mTorr. During the entire NH_3 plasma half-cycle, Ar continued to flow to the reaction chamber, and an additional 50 sccm of NH_3 was introduced 5 s prior to igniting the plasma to allow the chamber pressure to rise to 100 mTorr. The NH_3–Ar plasma half-reaction cycle was set to 45 s. The final step in the complete ALD cycle was a 10-s Ar purge step to remove the unreacted NH_3 from the chamber. Unless specified otherwise in the Results and Discussion section, the in situ infrared spectra were recorded as difference spectra, where a fresh background was collected prior a half-reaction cycle. The infrared data was recorded over a spectral range of 700 to 4000 cm^{-1} with a spectral resolution of 4 cm^{-1}. Each spectrum was averaged over 500–1000 scans.

Ex Situ Film Characterization. The SiN_x films for ex situ characterization were deposited in a test ALD reactor at Lam Research Corporation under conditions that were nominally similar to those described above. To determine the conformality, using the above SiN_x ALD process, we deposited a ~30 nm thick SiN_x film at 400 °C over high-aspect-ratio nanostructures with a width and height of ~100 and ~450 nm, respectively. To create these substrates, we deposited an SiO_2 film on a Si wafer using PECVD, and subsequently etched into nanostructures. The SiO_2 nanostructures were then coated with a SiN_x layer deposited by high-temperature CVD, onto which an SiO_2 thin film was deposited using ALD. The cross-sectional imaging of these SiN_x films deposited on the high-aspect-ratio nanostructures was performed on a JEOL 2010F ultrahigh-resolution scanning TEM at 200 kV. The SiN_x sample was coated with a layer of spin-on epoxy to protect the film from damage during sample preparation. The SiN_x sample was then attached onto a Cu TEM grid, after which it was milled, and polished using an ion beam at 30 kV, 100 pA; and 5 kV, 40 pA, respectively. RBS combined with HFS was used to determine the elemental composition of an SiN_x film deposited at 400 °C. The incident He^{2+} beam energy was 2.275 MeV and the ion beam was oriented at 75° with respect to the sample normal. The He^{2+} backscatter detector and the HFS detector were positioned at an angle of 160° and ~30°, respectively, with respect to the direction of the unscattered He^{2+} beam. The ellipsometry data was obtained using a single wavelength ellipsometer at an angle of 70° at 633 nm. The SiN_x films studied using ellipsometry were deposited with 500 ALD cycles at 400 °C.

3. RESULTS AND DISCUSSION

Figure 3 shows the infrared difference spectra for SiN_x films grown at 350, 400, and 450 °C for five complete Si_2Cl_6 and NH_3 plasma half-cycles. The primary infrared absorption band observed in Figure 3 corresponds to increase in absorbance for the Si–N–Si antisymmetric stretching mode[44] at ~875 cm^{-1} clearly indicating growth of SiN_x films over the entire temperature range of 350–450 °C. The band at ~1180 cm^{-1} was attributed to the NH bending mode in SiN_x,[45] while a very weak NH_2 scissor mode was observed at ~1550 cm^{-1}.[45,46] The corresponding NH_x (x = 1,2) stretching vibrations appeared at ~3300 cm^{-1}.[45] Absorbance due to the SiH_x (x = 1,2,3) stretching modes in SiN_x at ~2100–2200 cm^{-1},[44,47] was not observed in either of the three spectra in Figure 3. This indicates that in this ALD process for SiN_x, over the temperature range of 350–450 °C, almost all of the H in the films was essentially incorporated as –NH groups. A net incorporation of –NH into the film, indicates that complete ligand-exchange reactions do not occur in this SiN_x ALD process during the Si_2Cl_6 half-reaction cycle. In addition, the infrared spectra in Figure 3 show that as the deposition temperature was increased from 350 to 450 °C, the absorbance for the NH_x stretching mode decreased, indicating that less H was incorporated into the SiN_x films at higher deposition temperatures. This is consistent with the observation of Jang et al., who also showed that increasing the SiN_x growth temperature during ALD from $N(SiH_3)_3$ and NH_3 plasma resulted in a lower H concentration in the films.[36]

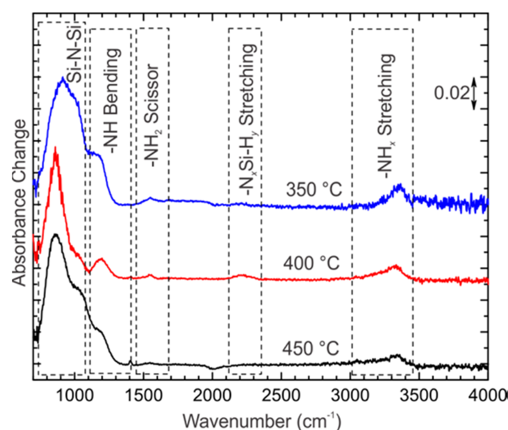

Figure 3. IR absorbance spectra for SiN_x films after five Si_2Cl_6 and NH_3 plasma ALD cycles at varying substrate temperatures. Absorbance due to the N–H bending mode decreases with increasing deposition temperature.

Figure 4 shows a TEM micrograph for a ~30 nm-thick SiN_x film deposited using the Si_2Cl_6 and NH_3 plasma ALD process onto an SiO_2-coated substrate. A comparison of the SiN_x film thickness on the sidewalls and the planar area in the nanostructured architecture shows that the SiN_x film had a conformality >95%. Thus, this ALD process can be potentially used for depositing highly conformal SiN_x films for semiconductor devices with high-aspect-ratio nanostructures.

Figure 5 shows the infrared difference spectra for the Si_2Cl_6 and NH_3 plasma half-cycles at (a) 400 °C and (b) 450 °C. During the Si_2Cl_6 half-cycle, the infrared difference spectra at both temperatures show an almost complete consumption of surface –NH_2 species indicated by a decrease in absorbance at ~1550 cm^{-1}, which is nearly identical to the increase in

DOI: 10.1021/acsami.5b01531
ACS Appl. Mater. Interfaces 2015, 7, 10806–10813

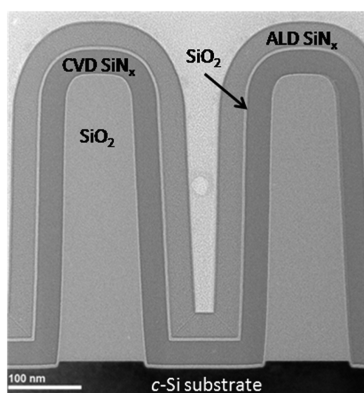

Figure 4. Cross-sectional transmission electron microscopy image of a conformal SiN_x film deposited on SiO_2 by ALD at 400 °C using Si_2Cl_6 and NH_3 plasma.

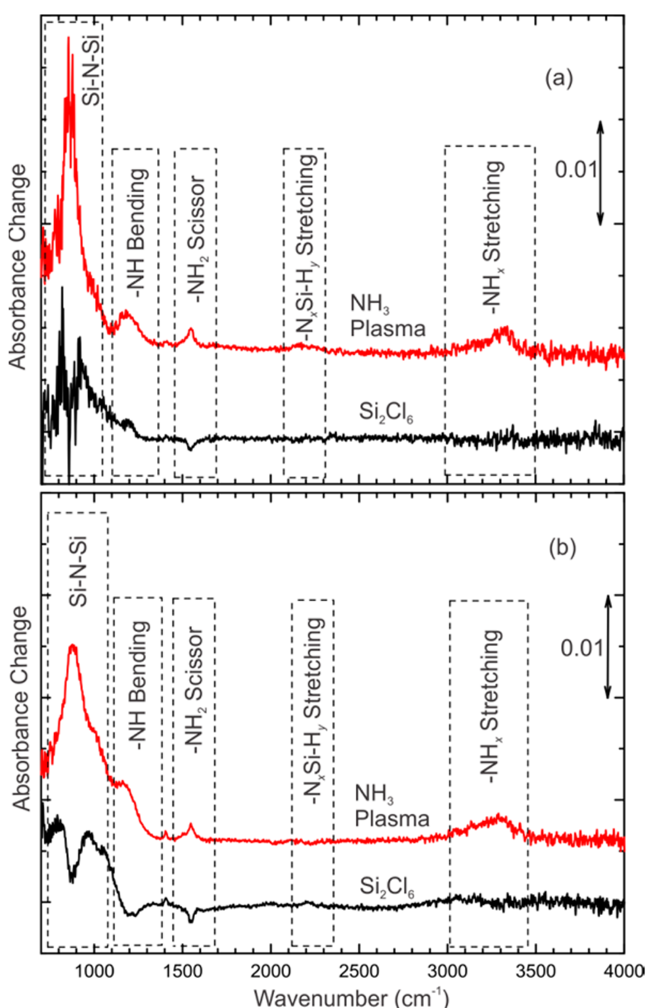

Figure 5. Infrared difference spectra for the Si_2Cl_6 and NH_3 plasma half-cycles at (a) 400 °C and (b) 450 °C.

absorbance for this mode during the NH_3 plasma half-cycle. Thus, surface $-NH_2$ groups created during the NH_3 plasma half-cycle are at least one of the reactive sites for Si_2Cl_6 chemisorption. Interestingly, at 400 °C, an increase in absorbance due to surface $-NH$ species was observed at $\sim$1180 cm^{-1} during the Si_2Cl_6 half-cycle even though there are no H atoms in this Si precursor. This indicates that Si_2Cl_6 reacted with surface $-NH_2$, abstracted a surface H atom to form surface $-NH$ species, and HCl was released into the gas phase as a reaction byproduct. In addition, once these surface $-NH$ groups were formed, they were unreactive to Si_2Cl_6 molecules at 400 °C. However, at 450 °C, a decrease in absorbance for the surface $-NH$ species was observed at $\sim$1180 cm^{-1}, suggesting that at the higher temperature, Si_2Cl_6 reacted with both $-NH$ and $-NH_2$ surface species. Therefore, $-NH_2$ groups on the SiN_x surface were more reactive to Si_2Cl_6 compared to surface $-NH$ groups. This observation in Figure 5 was also consistent with the infrared difference spectra for 5 complete ALD cycles in Figure 4, where based on the presence of the absorbance band at $\sim$1180 cm^{-1}, we concluded that a substantial fraction of $-NH$ groups (but with almost no $-NH_2$ groups) were incorporated within the growing SiN_x films. The absorbance increase in Figure 5 in the 875 cm^{-1} region during the NH_3 plasma half-cycle indicates a majority of Si$-$N$-$Si bonds were formed during this step. In fact, during the Si_2Cl_6 cycle, at both substrate temperatures, 400 and 450 °C, there was a decrease in the absorbance in the Si$-$N$-$Si region: this, in turn, suggests that chemisorption of Si_2Cl_6 was either accompanied by the breaking of Si$-$N$-$Si bonds or the chemisorption process influenced the infrared absorbance for the surface Si$-$N$-$Si bonds because of dielectric screening.[48−50]

Figure 6 shows the temporal evolution of the absorbance change during the NH_3 plasma half-cycle. In these experiments,

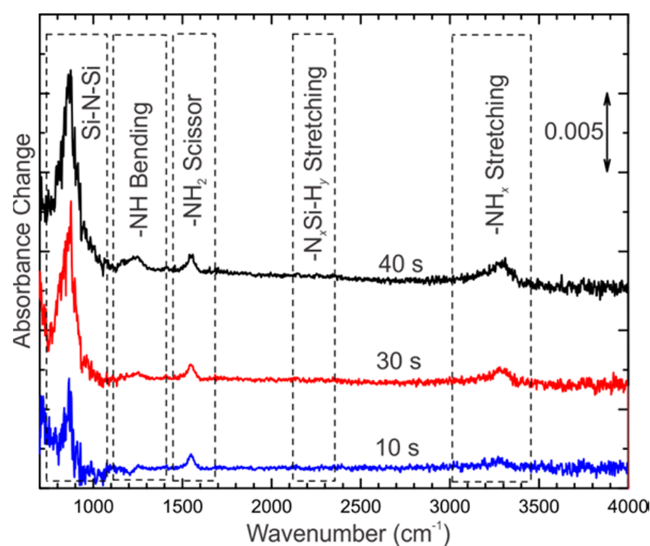

Figure 6. Temporal evolution of the infrared difference spectra at 400 °C during the NH_3 plasma half-cycle, showing saturation of the surface reactions.

the growing SiN_x surface was exposed to an NH_3 plasma immediately after an Si_2Cl_6 half-cycle, and infrared difference spectra were recorded after 10, 30, and 40 s with respect to the same reference spectrum. In the spectra in Figure 6, the change in absorbance from 30 to 40 s for the Si$-$N$-$Si antisymmetric stretching mode at $\sim$875 cm^{-1} was minimal, which confirmed SiN_x growth during the NH_3 plasma half-cycle was self-limiting. The surface $-NH_2$ species, which appear at $\sim$1550 cm^{-1}, were saturated after just 10 s of NH_3 plasma exposure. However, the absorbance due to $-NH$ species at $\sim$1180 cm^{-1} continued to increase gradually throughout the first 40 s of NH_3 plasma exposure, even after SiN_x film growth stopped at 30 s. We

DOI: 10.1021/acsami.5b01531
ACS Appl. Mater. Interfaces 2015, 7, 10806−10813

speculate that this increase in −NH absorbance was due to the incorporation of H atoms produced in the NH_3 plasma into the subsurface region of the SiN_x films. Since the duration of the NH_3 plasma may directly affect the H content of the film, it is critical that the NH_3 plasma exposure is no longer than necessary to obtain the maximum SiN_x film growth as indicated by the absorbance in the Si−N−Si stretching region at ~875 cm^{-1}.

Based on the observations in Figures 4−6, an overall surface reaction schematic for the ALD of SiN_x films from Si_2Cl_6 and NH_3 plasma is summarized in Figure 7. The proposed reaction

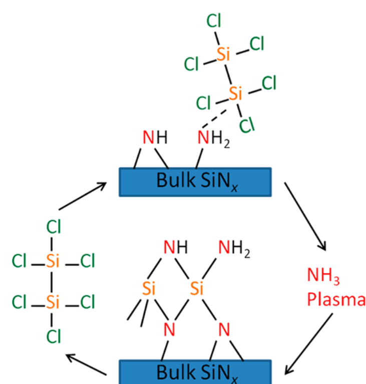

Figure 7. Proposed reaction schematic for SiN_x ALD using Si_2Cl_6 and NH_3 plasma.

pathway is similar to the one put forth by Murray et al. for the reaction of SiX_2H_2 molecules with an H-terminated Si_3N_4 surface, where X corresponds to a particular functional group.[26] On the basis of the density functional theory calculations of Murray et al., we propose that during the Si_2Cl_6 half-cycle, the Si_2Cl_6 molecules interact with surface $-NH_2$ group via overcoordination of a Si atom in Si_2Cl_6 with an N atom in the $-NH_2$ group. Murray et al. showed that this overcoordinated state for SiH_2X_2 molecules was energetically unfavorable, and based on their reaction schematic, we predict that this would result in the formation of surface $-Si_2Cl_5$ and −NH groups, with HCl as the byproduct which desorbs into the gas phase.[26] Several other authors have also suggested that generation of HCl was a pathway for the removal of Cl atoms from the growing SiN_x film.[27,28,33] The generation of HCl as a reaction byproduct can be indirectly verified by the formation of NH_4Cl due to subsequent reaction with NH_3. In some initial experiments, not reported in this manuscript, where the purge time between the half-reaction cycles was not sufficient, we did indeed observe vibrational modes corresponding to NH_4Cl in our infrared spectra. However, we do not expect this reaction to be relevant on the ZnSe IRC at temperatures ≥350 °C because NH_4Cl decomposes back to NH_3 and HCl at these temperatures. Therefore, we conclude that the most likely pathway for NH_4Cl formation in our initial experiments with lower purge time was on the cold walls of the chamber, which include the two KBr windows that are in the infrared beam path (see Figure 1). The purge conditions were subsequently modified to minimize NH_4Cl formation. Klaus et al. used transmission FTIR spectroscopy to show that $-SiCl_x$ (x = 1, 2, 3) groups were present on the growing SiN_x surface after $SiCl_4$ exposure.[28] While we expect similar surface species after the Si_2Cl_6 half-cycle, we were unable to detect these vibrational modes since $SiCl_x$ (x = 1, 2, 3) stretching vibrations appear at ~600−650 cm^{-1}, which is below the cutoff frequency for the MCT-A detector.

The chemical composition of SiN_x films, such as the N/Si ratio and the H content, strongly affects their properties.[36] The shape of the 700−1000 cm^{-1} absorption band, which corresponds to the Si−N−Si antisymmetric stretching phonon mode in SiN_x, strongly depends on the N/Si ratio. In general, this region can be deconvoluted into three distinct bands: ν_1, ν_2, and ν_3, each corresponding to a different local bonding environment within the broader Si−N−Si vibrational mode. The first band at ~790 cm^{-1}, designated as the ν_1, was originally attributed by Lucovsky et al. to a Si_3−Si-N antisymmetric stretching mode, corresponds to a Si-rich bonding environment.[44] However, Hasegawa et al. later showed that this mode may appear at a frequency as low as ~750 cm^{-1}.[44,51] The ν_2 band at ~875 cm^{-1} was attributed by Lucovsky et al. to the Si−N−Si antisymmetric stretching vibrations in stoichiometric SiN_x films.[44] Bandet et al. however attributed this mode to a feature at ~900 cm^{-1}.[52] The presence of a ν_3 band at >970 cm^{-1} was attributed by several authors to SiN_4 antisymmetric stretching vibrations in N-rich SiN_x films.[53,54] Lin and Lee also reported a shoulder at ~980 cm^{-1} for N-rich SiN_x films deposited at 300 °C, but this mode blue-shifted to 1070 cm^{-1} when the films were annealed from 300 to 800 °C.[55]

Figure 8 shows the 700−1000 cm^{-1} region for an SiN_x film grown at 400 °C using five complete Si_2Cl_6 and NH_3 plasma

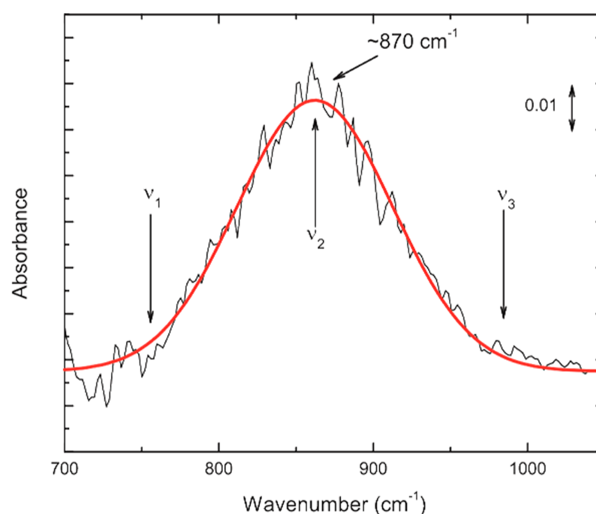

Figure 8. Deconvolution of the Si−N−Si phonon mode for an SiN_x film grown at 400 °C. The distinct bands, ν_1, ν_2, and ν_3, are required to account for different local bonding environments within SiN_x films.

ALD cycles. For our films, this region could be deconvoluted with a single Gaussian centered at ~870 cm^{-1}, which we attributed to as the ν_2 band. Since the ν_1 and ν_3 bands were absent in the Si−N−Si antisymmetric stretching region, Si- and N-rich domains were unlikely in these SiN_x films.

Table 1 shows the elemental composition of an SiN_x film grown using Si_2Cl_6 and NH_3 plasma at 400 °C obtained using RBS combined with HFS. There was a negligible concentration of Cl incorporated in the films, which is in agreement with other studies on SiN_x ALD using chlorosilanes.[27,28,33] Yokoyama et al. attributed the low Cl content in SiN_x films deposited using chlorosilanes and an NH_3 plasma to the H radicals generated in the plasma, which abstract surface Cl

DOI: 10.1021/acsami.5b01531
ACS Appl. Mater. Interfaces 2015, 7, 10806−10813

Table 1. Elemental Composition of an SiN_x Film Grown at 400 °C via ALD Using Si_2Cl_6 and an NH_3 Plasma Determined Using RBS Combined with HFS

element	atomic percent (%)
Si	28.0 ± 1.0
N	48.4 ± 3.0
H	23.3 ± 2.0
Cl	0.1 ± 0.05

atoms to form HCl.[33] The SiN_x film (see Table 1) however contained ~23 atomic % H atoms, which is typical of low-temperature SiN_x deposition processes.[34,56] The infrared difference spectra in Figure 3 show that the SiN_x films contained negligible fraction of H atoms as $-SiH_x$ (x = 1,2,3) or $-NH_2$ groups, and a majority of the H was present in the form of −NH groups. On the basis of the RBS/HFS data, the N/Si ratio in the films was ~1.7, which may appear to be in contradiction with the analysis of the infrared data in Figure 8 that showed that the SiN_x film did not contain N-rich regions with N−N bonds. If these −NH groups in the SiN_x films were hypothetically dehydrogenated by the restructuring of two adjacent Si-NH groups to form a Si−N−Si bridged structure, this would result in the removal of two H atoms for each N atom. Therefore, if we subtract half the H concentration (23%) from the observed N concentration (48.4%), the new N/Si ratio is ~1.31, which is close to the perfectly stoichiometric N/Si ratio of 1.33: this is in agreement with the analysis of the Si−N−Si asymmetric stretching mode, which predicts no N- or Si-rich regions with N−N or Si−Si bonds, respectively. The film density obtained from the RBS measurements was ~2.35 g/cm^3, which is much lower than ~3.2 g/cm^3 for stoichiometric Si_3N_4 deposited using high-temperature processes[57] but similar to the film densities reported for low-temperature SiN_x ALD processes.[25,33,34] We attribute the low density of the SiN_x films to the high level of H incorporation.

Figure 9 shows the GPC of an SiN_x film deposited at 400 °C using 500 complete ALD cycles as a function of Si_2Cl_6 dose.

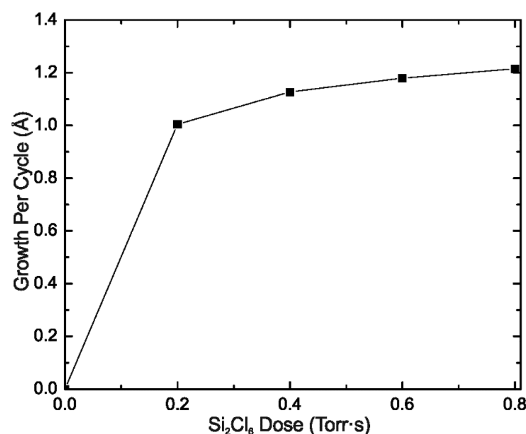

Figure 9. SiN_x GPC as a function of Si_2Cl_6 dose at 400 °C, keeping the NH_3 plasma half-cycle duration fixed.

The maximum GPC was ~1.2 Å at a Si_2Cl_6 exposure of ~8 × 10^5 L. The diminishing increase in GPC at doses >2 × 10^5 L indicates that the ALD process was self-limiting. The GPC of this SiN_x process was similar to that previously reported for the plasma and thermal ALD processes.[30,33,35] However, the Si precursor dose was ~1−4 orders of magnitude less than those reported for thermal SiN_x ALD processes, and ~1 order of magnitude less than those reported for plasma-assisted SiN_x ALD processes, with the exception of the plasma-assisted ALD process using $N(SiH_3)_3$ as the Si precursor. The refractive index of the film was ~1.9, which is similar to the reported refractive indices of SiN_x films deposited using other low-temperature ALD processes, but lower than the generally accepted value of ~2.0 for dense Si_3N_4 films.[32]

4. CONCLUSION

We have developed a novel process for the plasma-assisted ALD of SiN_x films over the substrate temperature range of 350−450 °C using Si_2Cl_6 and NH_3 plasma. These films show >95% conformality on patterned substrates with trenches that have an aspect ratio of ~5. Our infrared data show that during the ALD of SiN_x, Si_2Cl_6 reacted preferentially with surface $-NH_2$ compared to −NH groups. The reaction with surface $-NH_2$ groups led to the formation of −NH groups, which were eventually incorporated into the growing SiN_x film because of their lower reactivity with Si_2Cl_6. At a higher substrate temperature, 450 °C, Si_2Cl_6 also reacted with some surface −NH species, which led to a lower H content in the SiN_x films. Furthermore, over the range of temperatures explored, the infrared data show that a majority of the H atoms incorporated into the SiN_x film were present as −NH species. We also show that Si−N−Si bond formation occurs primarily during the NH_3 plasma half-cycle. Ellipsometry data shows that the SiN_x ALD process had a maximum GPC of 1.2 Å at 400 °C at an Si_2Cl_6 exposure of ~8 × 10^5 L, with a refractive index of ~1.9. RBS/HFS analysis shows that SiN_x films grown at 400 °C had ~23 atomic % H atoms with a density of 2.35 g/cm^3. Although the films were N-rich with an N/Si ratio of 1.71, this was primarily due to the presence of −NH groups.

AUTHOR INFORMATION

Corresponding Authors

*E-mail: sagarwal@mines.edu.

*E-mail: dennis.hausmann@lamresearch.com.

Notes

The authors declare no competing financial interest.

ACKNOWLEDGMENTS

The authors thank Lam Research Corporation for funding the project, Nanolabs for the TEM imaging, and Evans Analytical Group for the RBS/HFS analysis.

REFERENCES

(1) Miikkulainen, V.; Leskela, M.; Ritala, M.; Puurunen, R. L. Crystallinity of Inorganic Films Grown by Atomic Layer Deposition: Overview and General Trends. *J. Appl. Phys.* **2013**, *113*, 101.

(2) Puurunen, R. L. Surface Chemistry of Atomic Layer Deposition: A Case Study for the Trimethylaluminum/Water Process. *J. Appl. Phys.* **2005**, *97*, 52.

(3) George, S. M. Atomic Layer Deposition: An Overview. *Chem. Rev.* **2010**, *110*, 111−131.

(4) Bosund, M.; Mattila, P.; Aierken, A.; Hakkarainen, T.; Koskenvaara, H.; Sopanen, M.; Airaksinen, V. M.; Lipsanen, H. GaAs Surface Passivation by Plasma-Enhanced Atomic-Layer-Deposited Aluminum Nitride. *Appl. Surf. Sci.* **2010**, *256*, 7434−7437.

(5) Butcher, K. S. A.; Afifuddin, P.; Chen, P. T.; Godlewski, M.; Szczerbakow, A.; Goldys, E. M.; Tansley, T. L.; Freitas, J. A. Recrystallization Prospects for Freestanding Low-Temperature GaN Grown Using ZnO Buffer Layers. *J. Cryst. Growth* **2002**, *246*, 237−243.

DOI: 10.1021/acsami.5b01531
ACS Appl. Mater. Interfaces 2015, 7, 10806−10813

(6) Ferguson, J. D.; Weimer, A. W.; George, S. M. Atomic Layer Deposition of Boron Nitride Using Sequential Exposures of BCl_3 and NH_3. *Thin Solid Films* **2002**, *413*, 16−25.
(7) Ihanus, J.; Lankinen, M. P.; Kemell, M.; Ritala, M.; Leskela, M. Aging of Electroluminescent ZnS: Mn Thin Films Deposited by Atomic Layer Deposition Processes. *J. Appl. Phys.* **2005**, *98*, 113526.
(8) Juppo, M.; Ritala, M.; Leskela, M. Use of 1,1-Dimethylhydrazine in the Atomic Layer Deposition of Transition Metal Nitride Thin Films. *J. Electrochem. Soc.* **2000**, *147*, 3377−3381.
(9) Kattelus, H.; Ylilammi, M.; Saarilahti, J.; Antson, J.; Lindfors, S. Layered Tantalum-Aluminum Oxide-Films Deposited by Atomic Layer Epitaxy. *Thin Solid Films* **1993**, *225*, 296−298.
(10) Kim, Y. S.; Kang, J. S.; Yun, S. J.; Cho, K. I. Multilayered Tantalum-Aluminum Oxide Films Grown by Atomic Layer Deposition. *J. Korean Phys. Soc.* **1999**, *35*, S216−S220.
(11) Lu, J.; Sundqvist, J.; Ottosson, M.; Tarre, A.; Rosental, A.; Aarik, J.; Harsta, A. Microstructure Characterisation of ALD-Grown Epitaxial SnO_2 Thin Films. *J. Cryst. Growth* **2004**, *260*, 191−200.
(12) Luoh, T.; Su, C.-T.; Yang, T.-H.; Chen, K.-C.; Lu, C.-Y. Advanced Tungsten Plug Process for Beyond Nanometer Technology. *Microelectron. Eng.* **2008**, *85*, 1739−1747.
(13) Martinson, A. B. F.; Elam, J. W.; Pellin, M. J. Atomic Layer Deposition of Cu_2S for Future Application in Photovoltaics. *Appl. Phys. Lett.* **2009**, *94*, 123107.
(14) Pore, V.; Ritala, M.; Leskela, M. Atomic Layer Deposition of Titanium Disulfide Thin Films. *Chem. Vap. Deposition* **2007**, *13*, 163−168.
(15) Rossnagel, S. M.; Sherman, A.; Turner, F. Plasma-Enhanced Atomic Layer Deposition of Ta and Ti for Interconnect Diffusion Barriers. *J. Vac. Sci. Technol. B* **2000**, *18*, 2016−2020.
(16) Torndahl, T.; Ottosson, M.; Carlsson, J. O. Growth of Copper Metal by Atomic Layer Deposition Using Copper(I) Chloride, Water and Hydrogen as Precursors. *Thin Solid Films* **2004**, *458*, 129−136.
(17) Lin, H.; Xu, L. Q.; Chen, X.; Wang, X. H.; Sheng, M.; Stubhan, F.; Merkel, K. H.; Wilde, J. Moisture-Resistant Properties of SiN_x Films Prepared by PECVD. *Thin Solid Films* **1998**, *333*, 71−76.
(18) Kim, J. S.; Kwon, B. S.; Heo, W.; Jung, C. R.; Park, J. S.; Shon, J. W.; Lee, N. E. Highly Selective Etching of Silicon Nitride to Physical-Vapor-Deposited *a*-C Mask in Dual-Frequency Capacitively Coupled CH_2F_2/H_2 Plasmas. *J. Vac. Sci. Technol. A* **2010**, *28*, 65−68.
(19) Lauinger, T.; Schmidt, J.; Aberle, A. G.; Hezel, R. Record Low Surface Recombination Velocities on 1 Ω cm *p*-silicon Using Remote Plasma Silicon Nitride Passivation. *Appl. Phys. Lett.* **1996**, *68*, 1232−1234.
(20) Nakayama, D.; Wada, A.; Kubota, T.; Bruce, R.; Martin, R. M.; Haass, M.; Fuller, N.; Samukawa, S. Highly Selective Silicon Nitride Etching to Si and SiO_2 for a Gate Sidewall Spacer Using a $CF_3I/O_2/H_2$ Neutral Beam. *J. Phys. D: Appl. Phys.* **2013**, *46*, 205203.
(21) Holt, J. K.; Goodwin, D. G.; Gabor, A. M.; Jiang, F.; Stavola, M.; Atwater, H. A. Hot-Wire Chemical Vapor Deposition of High Hydrogen Content Silicon Nitride for Solar Cell Passivation and Anti-Reflection Coating Applications. *Thin Solid Films* **2003**, *430*, 37−40.
(22) Kim, K.; Dhungel, S. K.; Yoo, J.; Jung, S.; Mangalaraj, D.; Yi, J. Hydrogenated Silicon-Nitride Thin Films as Antireflection and Passivation Coatings for Multicrystalline Silicon Solar Cells. *J. Korean Phys. Soc.* **2007**, *51*, 1659−1662.
(23) Aberle, A. G. Overview on SiN Surface Passivation of Crystalline Silicon Solar Cells. *Sol. Energy Mater. Sol. Cells* **2001**, *65*, 239−248.
(24) Suchaneck, G.; Norkus, V.; Gerlach, G. Low-Temperature PECVD-Deposited Silicon Nitride Thin Films for Sensor Applications. *Surf. Coat. Technol.* **2001**, *142*, 808−812.
(25) King, S. W. Plasma Enhanced Atomic Layer Deposition of SiN_x:H and SiO_2. *J. Vac. Sci. Technol. A* **2011**, *29*, 041501.
(26) Murray, C. A.; Elliott, S. D.; Hausmann, D.; Henri, J.; LaVoie, A. Effect of Reaction Mechanism on Precursor Exposure Time in Atomic Layer Deposition of Silicon Oxide and Silicon Nitride. *ACS Appl. Mater. Interfaces* **2014**, *6*, 10534−10541.
(27) Morishita, S.; Sugahara, S.; Matsumura, M. Atomic-Layer Chemical-Vapor-Deposition of Silicon-Nitride. *Appl. Surf. Sci.* **1997**, *112*, 198−204.
(28) Klaus, J. W.; Ott, A. W.; Dillon, A. C.; George, S. M. Atomic Layer Controlled Growth of Si_3N_4 Films Using Sequential Surface Reactions. *Surf. Sci.* **1998**, *418*, L14−L19.
(29) Nakajima, A.; Yoshimoto, T.; Kidera, T.; Yokoyama, S. Low-Temperature Formation of Silicon Nitride Gate Dielectrics by Atomic-Layer Deposition. *Appl. Phys. Lett.* **2001**, *79*, 665−667.
(30) Lee, W. J.; Lee, J. H.; Park, C. O.; Lee, Y. S.; Shin, S. J.; Rha, S. K. A Comparative Study on the Si Precursors for the Atomic Layer Deposition of Silicon Nitride Thin Films. *J. Korean Phys. Soc.* **2004**, *45*, 1352−1355.
(31) Zhu, S.; Nakajima, A. Atomic Layer Deposition of HfO_2 and Si Nitride on Ge Substrates. *Jpn. J. Appl. Phys., Part 1* **2007**, *46*, 7699−7701.
(32) Park, K.; Yun, W.-D.; Choi, B.-J.; Kim, H.-D.; Lee, W.-J.; Rha, S.-K.; Park, C. O. Growth Studies and Characterization of Silicon Nitride Thin Films Deposited by Alternating Exposures to Si_2Cl_6 and NH_3. *Thin Solid Films* **2009**, *517*, 3975−3978.
(33) Yokoyama, S.; Goto, H.; Miyamoto, T.; Ikeda, N.; Shibahara, K. Atomic Layer Controlled Deposition of Silicon Nitride and in Situ Growth Observation by Infrared Reflection Absorption Spectroscopy. *Appl. Surf. Sci.* **1997**, *112*, 75−81.
(34) Goto, H.; Shibahara, K.; Yokoyama, S. Atomic Layer Controlled Deposition of Silicon Nitride with Self-Limiting Mechanism. *Appl. Phys. Lett.* **1996**, *68*, 3257−3259.
(35) Yokoyama, S.; Ikeda, N.; Kajikawa, K.; Nakashima, Y. Atomic-Layer Selective Deposition of Silicon Nitride on Hydrogen-Terminated Si Surfaces. *Appl. Surf. Sci.* **1998**, *130*, 352−356.
(36) Jang, W.; Jeon, H.; Kang, C.; Song, H.; Park, J.; Kim, H.; Seo, H.; Leskela, M.; Jeon, H. Temperature Dependence of Silicon Nitride Deposited by Remote Plasma Atomic Layer Deposition. *Phys. Status Solidi A* **2014**, *211*, 2166−2171.
(37) Rai, V. R.; Agarwal, S. In Situ Diagnostics for Studying Gas-Surface Reactions During Thermal and Plasma-Assisted Atomic Layer Deposition. *J. Vac. Sci. Technol. A* **2012**, *30*, 01A158.
(38) Chabal, Y. J. Surface Infrared Spectroscopy. *Surf. Sci. Rep.* **1988**, *8*, 211−357.
(39) Rai, V. R.; Agarwal, S. Surface Reaction Mechanisms During Ozone-Based Atomic Layer Deposition of Titanium Dioxide. *J. Phys. Chem. C* **2008**, *112*, 9552−9554.
(40) Rai, V. R.; Agarwal, S. Surface Reaction Mechanisms During Plasma-Assisted Atomic Layer Deposition of Titanium Dioxide. *J. Phys. Chem. C* **2009**, *113*, 12962−12965.
(41) Rai, V. R.; Agarwal, S. Mechanism of Self-Catalytic Atomic Layer Deposition of Silicon Dioxide Using 3-Aminopropyl Triethoxysilane, Water, and Ozone. *Chem. Mater.* **2011**, *23*, 2312.
(42) Rai, V. R.; Vandalon, V.; Agarwal, S. Surface Reaction Mechanisms During Ozone and Oxygen Plasma Assisted Atomic Layer Deposition of Aluminum Oxide. *Langmuir* **2010**, *26*, 13732−13735.
(43) Rai, V. R.; Vandalon, V.; Agarwal, S. Influence of Surface Temperature on the Mechanism of Atomic Layer Deposition of Aluminum Oxide Using an Oxygen Plasma and Ozone. *Langmuir* **2012**, *28*, 350−357.
(44) Lucovsky, G.; Yang, J.; Chao, S. S.; Tyler, J. E.; Czubatyj, W. Nitrogen-Bonding Environments in Glow-Discharge-Deposited *a*-Si:H Films. *Phys. Rev. B* **1983**, *28*, 3234−3240.
(45) Tsu, D. V.; Lucovsky, G.; Mantini, M. J. Local Atomic-Structure in Thin-Films of Silicon Nitride and Silicon Diimide Produced by Remote Plasma-Enhanced Chemical-Vapor Deposition. *Phys. Rev. B* **1986**, *33*, 7069−7076.
(46) Colaianni, M. L.; Chen, P. J.; Yates, J. T. The Stepwise Dissociation of NH_3 on the Si(111)-(7 × 7) Surface - Low-Temperature Dissociative Adsorption and Thermal Effects. *J. Chem. Phys.* **1992**, *96*, 7826−7837.

DOI: 10.1021/acsami.5b01531
ACS Appl. Mater. Interfaces 2015, 7, 10806−10813

(47) Lucovsky, G. Chemical Effects on the Frequencies of Si-H Vibrations in Amorphous Solids. *Solid State Commun.* **1979**, *29*, 571−576.
(48) Dai, M.; Kwon, J.; Halls, M. D.; Gordon, R. G.; Chabal, Y. J. Surface and Interface Processes During Atomic Layer Deposition of Copper on Silicon Oxide. *Langmuir* **2010**, *26*, 3911−3917.
(49) Kwon, J.; Dai, M.; Halls, M. D.; Chabal, Y. J. Detection of a Formate Surface Intermediate in the Atomic Layer Deposition of High-κ Dielectrics Using Ozone. *Chem. Mater.* **2008**, *20*, 3248−3250.
(50) Sperling, B. A.; Kimes, W. A.; Maslar, J. E. Reflection Absorption Infrared Spectroscopy During Atomic Layer Deposition of HfO_2 Films from Tetrakis(Ethylmethylamido)Hafnium and Water. *Appl. Surf. Sci.* **2010**, *256*, 5035−5041.
(51) Hasegawa, S.; Anbutsu, H.; Kurata, Y. Connection between Si-N and Si-H Vibrational Properties in Amorphous SiN_x:H Films. *Philos. Mag. B* **1989**, *59*, 365−375.
(52) Bandet, J.; Despax, B.; Caumont, M. Nitrogen Bonding Environments and Local Order in Hydrogenated Amorphous Silicon Nitride Films Studied by Raman Spectroscopy. *J. Appl. Phys.* **1999**, *85*, 7899−7904.
(53) Scardera, G.; Puzzer, T.; Conibeer, G.; Green, M. A. Fourier Transform Infrared Spectroscopy of Annealed Silicon-Rich Silicon Nitride Thin Films. *J. Appl. Phys.* **2008**, *104*, 7.
(54) Bustarret, E.; Bensouda, M.; Habrard, M. C.; Bruyere, J. C.; Poulin, S.; Gujrathi, S. C. Configurational Statistics in a-$Si_xN_yH_z$ Alloys A Quantitative Bonding Analysis. *Phys. Rev. B* **1988**, *38*, 8171−8184.
(55) Lin, K. C.; Lee, S. C. The Structural and Optical-Properties of *a*-SiN_x:H Prepared by Plasma-Enhanced Chemical-Vapor Deposition. *J. Appl. Phys.* **1992**, *72*, 5474−5482.
(56) Lavareda, G.; de Carvalho, C. N.; Amaral, A.; Fortunato, E.; Ramos, A. R.; da Silva, M. E. Dependence of TFT Performance on the Dielectric Characteristics. *Thin Solid Films* **2003**, *427*, 71−76.
(57) Riley, F. L. Silicon Nitride and Related Materials. *J. Am. Ceram. Soc.* **2000**, *83*, 245−265.

DOI: 10.1021/acsami.5b01531
ACS Appl. Mater. Interfaces 2015, 7, 10806−10813